

Identifying Non-Abelian Topological Order through Minimal Entangled States

W. Zhu¹, S. S. Gong¹, F. D. M. Haldane², D. N. Sheng¹

¹*Department of Physics and Astronomy, California State University, Northridge, California 91330, USA and*

²*Department of Physics, Princeton University, Princeton, NJ 08544, USA*

The topological order is equivalent to the pattern of long-range quantum entanglements, which cannot be measured by any local observable. Here we perform an exact diagonalization study to establish the non-Abelian topological order through entanglement entropy measurement. We focus on the quasiparticle statistics of the non-Abelian Moore-Read and Read-Rezayi states on the lattice boson models. We identify multiple independent minimal entangled states (MESs) in the groundstate manifold on a torus. The extracted modular \mathcal{S} matrix from MESs faithfully demonstrates the Majorana quasiparticle or Fibonacci quasiparticle statistics, including the quasiparticle quantum dimensions and the fusion rules for such systems. These findings support that MESs manifest the eigenstates of quasiparticles for the non-Abelian topological states and encode the full information of the topological order.

PACS numbers: 73.43.Cd, 03.65.Ud, 05.30.Pr

Introduction.— One of the most striking phenomena in the fractional quantum Hall (FQH) system is the emergent fractionalized quasiparticles obeying Abelian [1] or non-Abelian [2–4] braiding statistics. Interchange of two Abelian quasiparticles leads to a nontrivial phase acquired by their wavefunction, whereas interchange of two non-Abelian quasiparticles results in an operation of matrix to the degenerating ground-state space and the final state will depend on the order of operations being carried out. The non-Abelian quasiparticles and its braiding statistics are fundamentally important for understanding the topological order and also have potential application in topologically fault-tolerant quantum computation [5–7]. So far, such quasiparticles have not been definitely identified in nature. However, it is generally believed that they exist in the FQH systems at filling factor $\nu = 5/2$ [8] and $12/5$ [9], described by the Moore-Read (MR) [2, 10, 11] and Read-Rezayi (RR) states [4, 12], respectively. The topological band model for optical lattices with bosonic particles is another promising platform to realize the non-Abelian topological states [13–23]. In the MR and RR states, the quasiparticles satisfy the following characteristic fusion rules that specify how the quasiparticles combine and fuse into more than one type of quasiparticles [7]:

$$MR: \quad \sigma \times \sigma = \mathbb{1} + \psi, \quad (1a)$$

$$RR: \quad \tau \times \tau = \mathbb{1} + \tau \quad (1b)$$

where $\mathbb{1}$ represents the identity particle, ψ the fermion-type quasiparticle, σ the Majorana quasiparticle and τ the Fibonacci quasiparticle. In general, the fusion rule of quasiparticles is encoded in the modular \mathcal{S} matrix through Verlinde formula [24–32]. Moreover, $\mathcal{S}(\mathcal{S}_{i1} = d_i/\mathcal{D})$ also determines the quasiparticle's individual quantum dimension (d_i) and total quantum dimension ($\mathcal{D} = \sqrt{\sum_i d_i^2}$) [33, 34]. Therefore, the \mathcal{S} matrix plays the central role in identifying topological order and corresponding quasiparticle statistics [29–32].

While the Berry phase and non-Abelian information of quasiparticles moving adiabatically around each other have been studied numerically [35–41], the full modular \mathcal{S} matrix and the corresponding fusion rules for the microscopic

models hosting the non-Abelian topological states have been lacking, due to the computational difficulty of directly dealing with and distinguishing different quasiparticles. Recently, there is growing interest on characterizing topological order through the quantum entanglement information [33, 34, 42–50]. Among the recent progresses, the relationship between the entanglement measurement and the modular matrix for topological nontrivial systems has been uncovered [47], which may open a new avenue to this challenging issue. The modular matrix and corresponding quasiparticle statistics have been successfully extracted through the MESs for chiral spin liquid and the Abelian FQH states [47, 48, 51], which serve as direct evidences that the MES is the eigenstate of the Wilson loop operators with a definite type of quasiparticle [44, 47, 48]. For non-Abelian case, it is more challenging as the quasiparticles usually have different quantum dimensions and topological entanglement entropies, and it is unclear if the MESs still represent the quasiparticle eigenstates. A recent variational quantum Monte Carlo calculation studied the quasiparticle statistics for a projected wavefunction [52], however the obtained result does not accurately reproduce the known modular matrix including each quasiparticle quantum dimension for the MR state; thus it is of critical importance to clarify if the MESs can lead to the accurate identification of the modular matrix and the corresponding topological order for microscopic non-Abelian quantum states.

In this letter, we present an exact diagonalization (ED) study of quasiparticle statistics of the possible MR and RR non-Abelian states through extracting the modular \mathcal{S} matrix for topological flat-band models [16–22] with bosonic particles at filling numbers $\nu = 1$ and $\nu = 3/2$. We map out the entanglement entropy profile for superposition states of the near degenerating groundstates and identify the global MES. We find that all other MESs can be obtained in the state space which is orthogonal to the global MES. The obtained MESs form the orthogonal and complete basis states for the modular transformation. We extract the modular \mathcal{S} matrix and establish the corresponding fusion rules, which unambiguously demonstrate the Majorana and Fibonacci quasiparticles emerging in

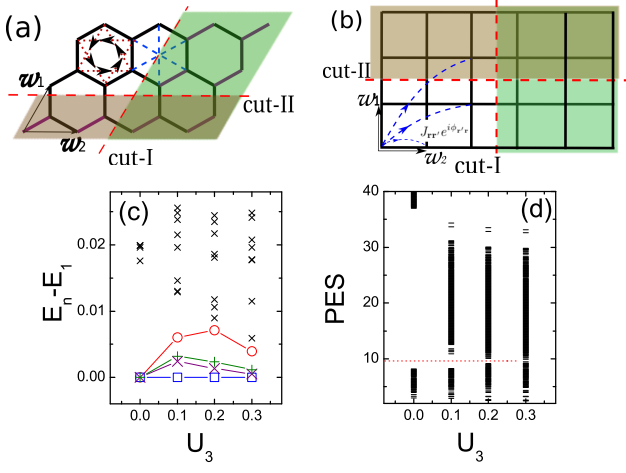


FIG. 1: (Color online) (a) Haldane model on HC lattice. The red dashed and blue dashed line represents the second NN hopping and third NN hopping, respectively. (b) SQ lattice with long-range hopping $J_{\mathbf{r}\mathbf{r}'} e^{i\phi_{\mathbf{r}\mathbf{r}'}}$ as shown by blue dashed line. (c) Low-energy spectrum $E_n - E_1$ versus the U_3 ($U_2 = 0, U_4 = \infty$) on a 4×4 SQ lattice at $\nu = 3/2$. Four lowest eigenvalues are labeled by blue square, purple cross, green cross and red circle. (d) Particle Entanglement Spectrum (PES) for tracing out 4 bosons. There are 298 states below the PES gap (red dashed line) for $U_3 < 0.3$, in good agreement with the counting of quasiparticle excitations in RR state.

these systems. We demonstrate that the obtained modular matrix as a topological invariant [31] of the system remains to be universal in the whole topological phase until a quantum phase transition takes place.

We study the lattice boson model with longer-range hoppings, which can be generally written as

$$H = \sum_{\mathbf{r}\mathbf{r}'} \left[J_{\mathbf{r}\mathbf{r}'} e^{i\phi_{\mathbf{r}\mathbf{r}'}} b_{\mathbf{r}}^\dagger b_{\mathbf{r}'} + \text{H.c.} \right] + \sum_n \frac{U_n}{n!} \sum_{\mathbf{r}} (b_{\mathbf{r}}^\dagger)^n (b_{\mathbf{r}})^n \quad (2)$$

where $b_{\mathbf{r}}^\dagger (b_{\mathbf{r}})$ creates (annihilates) a boson at site $\mathbf{r} = (x, y)$. U_n is an on-site N -body repulsive interaction. Here we consider two representative lattice models: the Haldane model on the honeycomb (HC) lattice [15, 16] and topological flat band model on the square (SQ) lattice [17]. On the HC lattice, we include up to the third nearest-neighbor (NN) hopping and a non-zero ϕ_{ij} on the second NN hopping only (the net flux is zero in one unit cell), as shown in Fig. 1(a). The NN hopping is set to be $J_{\mathbf{r}\mathbf{r}'} = 1$ and the other parameters are defined the same as in Ref. [15]. On the SQ lattice [17], we select the phase factor $\phi_{\mathbf{r}\mathbf{r}'}$ corresponding to half flux quanta per plaquette. The amplitude of hopping satisfies a particular gaussian form: $J_{\mathbf{r}\mathbf{r}'} = -tG(\mathbf{r} - \mathbf{r}') e^{-\frac{t}{4}|\mathbf{r}-\mathbf{r}'|^2}$, where $G(\mathbf{r} - \mathbf{r}') = (-1)^{(1+x-x')(1+y-y')}$ and $t = 1$ as the energy scale here. For both models, we consider a finite size system with $N_x \times N_y$ unit cells, the filling factor of lower band is $\nu = N_p/N_s$, where N_p is boson number and N_s is number of single-particle states in the flat band.

We first obtain the low energy spectrum of the SQ model at

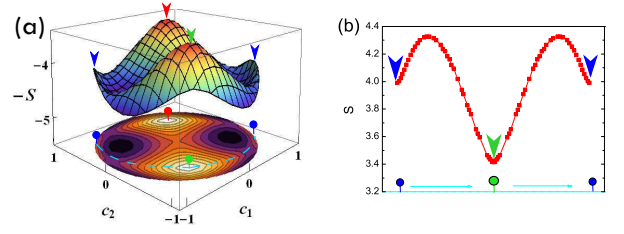


FIG. 2: (Color online) (a) Surface and contour plots of entanglement entropy ($-S$) of $|\Psi_{c_1, c_2, \phi_2, \phi_3}\rangle$ on 3×4 HC lattice at $\nu = 1$. We show entropy profile versus c_1, c_2 ($c_3 = \sqrt{1 - c_1^2 - c_2^2}$) by setting optimized $\phi_2^o = 1.26\pi$, $\phi_3^o = 0.40\pi$. Three nearly orthogonal MESs are marked by red, green and blue arrows (dots) in surface (contour) plot. The cyan dashed line represents the states orthogonal to the first MES (red dot). (b) Entropy for the states along the cyan dashed line as shown in (a). All calculations are for partition along cut-I.

filling number $\nu = 3/2$ and $\nu = 1$ (see [53]). For $\nu = 3/2$, we set $U_4 = \infty$ so that only three bosons can go to the same lattice site, which is effectively equivalent to a spin- $\frac{3}{2}$ system. Due to much larger Hilbert space than the conventional hardcore boson systems, the largest size we can deal with is limited to 4×4 for $\nu = 3/2$. We find strong numerical evidence of a possible $\nu = 3/2$ RR state and $\nu = 1$ MR state (see [53]) on the SQ lattice. As shown in the Fig. 1(c-d), at smaller U_3 side, we find robust fourfold degeneracy of groundstates on a torus and the right counting rule of quasiparticle excitations for RR state [54]. The $\nu = 1$ bosonic MR state on the HC lattice has also been identified in the previous study [15]. Here our focus is to characterize the quasiparticle statistics of the above non-Abelian states through calculating the modular S matrix.

To address the quasiparticle statistics, we first obtain the quasiparticle eigenstates through determining the MESs on a torus [47]. The entanglement entropy is defined as $S = -\text{Tr} \rho_A \log \rho_A$, where the reduced density matrix ρ_A is obtained through partitioning the full system into two subsystems A and B and tracing out the subsystem B . Here we consider two noncontractible bipartitions on torus geometry (cut-I and cut-II) (Fig. 1(a-b)), which is along the lattice vectors w_1, w_2 , respectively.

Moore-Read state at $\nu = 1$.— We denote the three groundstates from ED calculation as $|\xi_j\rangle$, (with $j = 1, 2, 3$) [15]. Now we form the general superposition states as,

$$|\Psi_{(c_1, c_2, \phi_2, \phi_3)}\rangle = c_1 |\xi_1\rangle + c_2 e^{i\phi_2} |\xi_2\rangle + c_3 e^{i\phi_3} |\xi_3\rangle$$

where $c_1, c_2, c_3, \phi_2, \phi_3$ are real superposition parameters. For each state $|\Psi\rangle$, we construct the reduced density matrix and obtain the corresponding entanglement entropy. We optimize values of $c_i \in [0, 1]$ and $\phi_i \in [0, 2\pi]$ to minimize the entanglement entropy. In Fig. 2(a), we show the entropy profile at optimized parameters (ϕ_2^o, ϕ_3^o) for MESs on the HC lattice. Here we draw the $-S$ in the surface and contour plots so that the peaks in entropy show up clearly representing the minimums of S . In Fig. 2(a), we find several peaks (entropy valleys) in $c_1 - c_2$ space. The first peak (red arrow) relates to

TABLE I: Entropy of MESs for $\nu = 1$ and $\nu = 3/2$. S_i represents the entropy of i -th MES. For $\nu = 1$, we use $\delta S = S_3 - (S_2 + S_1)/2$. For $\nu = 3/2$, $\delta S = (S_3 + S_4)/2 - (S_1 + S_2)/2$. δS^* is analytic prediction [33].

ν	lattice size	S_1	S_2	S_3	S_4	δS	δS^*	$\delta S/\delta S^*$
1	HC 3×4	3.416	3.416	3.991	-	0.576	0.693	0.831
1	SQ 4×4	2.546	2.924	3.357	-	0.622	0.693	0.897
1	SQ 4×6	2.528	2.971	3.443	-	0.694	0.693	1.001
$\frac{3}{2}$	SQ 4×4	3.168	3.732	4.157	4.417	0.837	0.961	0.871

the first (global) MES $|\Xi_1^I\rangle$. After determining $|\Xi_1^I\rangle$, we search for the states with minimal entropy in the state space orthogonal to $|\Xi_1^I\rangle$ as shown in Fig. 2(b). The second and the third MESs are shown by green and blue arrows (the two states labeled by blue arrows are equivalent), which are separately located in different entropy valleys as shown in Fig. 2(a). We find that the first two MESs have almost the same entropy value, indicating they are indeed topological equivalent with the same quantum dimension. We calculate the entropy difference δS between the third MES and the average of first two MES to extract the information of the quantum dimension of the third quasiparticle. As listed in Table-I, nonzero $\delta S \approx 0.576$ implies the quantum dimension $d > 1$ for the third quasiparticle state [33, 34], in agreement with the theoretical expectation for a MR state. We also search for MESs for SQ lattice [53] and find similar results as listed in Table-I.

To extract the topological information of the quantum states from MESs, we obtain the overlap between the MESs for two noncontractible partition directions, which gives rise to the modular matrix $S = \langle \Xi^I | \Xi^I \rangle$ [47]:

$$S \approx \frac{1}{2.033} \begin{pmatrix} 1.000 & 1.026 & 1.441 \\ 1.000 & 1.026 & -1.441 \\ 1.463 & -1.409 & 0.000 \end{pmatrix} \quad (3)$$

for the HC lattice and we find very similar result for the SQ lattice [53]. Both results are quite close to the theoretical result for MR state based on $SU(2)_2$ Chern-Simons theory [26–

28]: $S = \frac{1}{2} \begin{pmatrix} 1 & 1 & \sqrt{2} \\ 1 & 1 & -\sqrt{2} \\ \sqrt{2} & -\sqrt{2} & 0 \end{pmatrix}$, which determines the

quasiparticle quantum dimension as: $d_{\mathbb{1}} = 1, d_{\psi} = 1, d_{\sigma} = \sqrt{2}$, $\mathcal{D} = 2$ and non-trivial fusion rule in Eq. (1a). From Eq. (3), we obtain $d_{\sigma}^{HC} \approx 1.463$, $\mathcal{D}^{HC} \approx 2.033$ for the HC lattice (and $d_{\sigma}^{SQ} \approx 1.392$, $\mathcal{D}^{SQ} \approx 1.961$ for the SQ lattice [53]). Another striking point is that $S_{33} \sim 0$, which indicates that the two σ quasiparticles annihilate each other and fuse into different quasiparticles. To demonstrate this non-trivial behavior, we extract the fusion rule related to the third quasiparticle from the numerical S matrix through Verlinde formula [24] $a \times b = \sum_c N_{ab}^c c$ where $N_{ab}^c = \sum_m S_{am} S_{bm} S_{mc}^* / S_{1m}$:

$$HC: \quad \sigma \times \sigma \approx 1.005\mathbb{1} + 1.056\psi + 0.096\sigma \quad (4a)$$

$$SQ: \quad \sigma \times \sigma \approx 0.951\mathbb{1} + 0.959\psi + 0.004\sigma \quad (4b)$$

, which agrees excellently with the fusion rule of the MR state (Eq. 1a). Both the $d_{\sigma} \approx \sqrt{2}$ and the characteristic fusion rule Eq. (4a-4b) unambiguously demonstrate the third quasiparticle σ representing a Majorana fermion. The fusion rule represents two ways to fuse two Majorana quasiparticles therefore each pair of Majorana quasiparticles can act as a qubit for quantum computation [7].

Read-Rezayi State at $\nu = 3/2$.— We turn to study the possible non-Abelian phase at $\nu = 3/2$ and detect the Fibonacci quasiparticle statistics emerging in this state. Following the similar route for MR at $\nu = 1$, we search for the MESs in the space of the groundstate manifold using the following general wavefunctions:

$$|\Psi\rangle = c_1|\xi_1\rangle + c_2e^{i\phi_2}|\xi_2\rangle + c_3e^{i\phi_3}|\xi_3\rangle + c_4e^{i\phi_4}|\xi_4\rangle$$

where c_i and ϕ_i are the superposition parameters and $|\xi_j\rangle$ ($j = 1, 2, 3, 4$) are four groundstates from ED calculation. We optimize the superposition parameters c_i, ϕ_i to minimize the entanglement entropy. In Fig. 3(a), we show the global MES $|\Xi_1^I\rangle$ in parameter space as labeled by the black arrow. The other MESs $|\Xi_i^I\rangle$ ($i = 2, 3, 4$) are determined in the parameter space orthogonal to $|\Xi_1^I\rangle$ (Fig. 3(b)). The entropies of the last two MESs are different from the lowest two MESs as list in Table-I, which is consistent with the non-Abelian behavior of the quasiparticles. However, we also notice some finite size effect as all the four entropies are different.

For the $\nu = 3/2$ bosonic RR state, the edge conformal field theory is captured by the $SU(2)_3$ Wess-Zumino-Witten model [26, 28–30], whose modular matrix can be effectively described by a non-Abelian $k = 3 \mathbb{Z}_k$ -parafermion part coupled by an Abelian semion part as: $S = S_{pf} \otimes S_{U(1)} = \frac{1}{\sqrt{2+\phi}} \begin{pmatrix} 1 & \phi \\ \phi & -1 \end{pmatrix} \otimes \frac{1}{\sqrt{2}} \begin{pmatrix} 1 & 1 \\ 1 & -1 \end{pmatrix}$, where $\phi = \frac{1+\sqrt{5}}{2}$ is golden ratio number. As a comparison, we obtain the numerical modular matrix by calculating the overlap between the

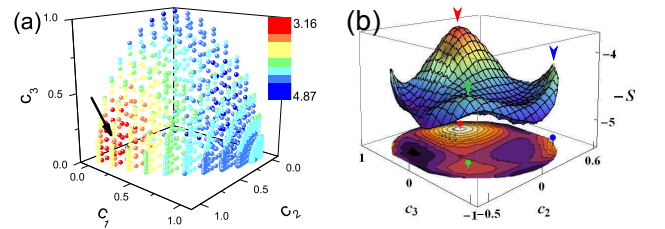


FIG. 3: (Color online) (a) The entropy profile of wavefunction $|\Psi\rangle$ at $\nu = 3/2$ in $c_1 - c_2 - c_3$ space by setting optimized $\phi_2^o = 0.90\pi, \phi_3^o = 0.46\pi, \phi_4^o = 0.68\pi$. The color of dots represents the magnitude of entropy. The first MES indicated by black arrow. (b) The entropy profile versus $c_2 - c_3$ in the space orthogonal to the first MES. The second, third and fourth MESs are labeled by red, green and blue arrows and dots, respectively. The calculation is for bipartition system along cut-I direction.

MESs along cut I and II:

$$\mathcal{S} \approx \mathcal{S}_{pf} \otimes \mathcal{S}_{U(1)} + 10^{-2} \times \begin{pmatrix} 4.3 & -3.4 & -0.4 & 1.1 \\ -2.7 & -3.1 & -0.9 & -0.1 \\ 2.1 & -0.8 & 2.4 & -0.7 \\ 0.0 & -1.0 & -0.1 & -1.9 \end{pmatrix} \quad (5)$$

, which agrees with the analytic prediction (with a finite size correction of the order of 10^{-2}). The modular matrix \mathcal{S}_{pf} signals Fibonacci quasiparticle including the quantum dimension $d_\tau = \phi \approx 1.618$ and the related fusion rule as shown in Eq. (1b). Two Fibonacci quasiparticles may fuse into an identity or a Fibonacci quasiparticle, which is analogous to two $SU(2)$ spin-1/2's combining to either spin-1 or spin-0 total spin [55]. Using this property, Fibonacci quasiparticles is capable of universal topological quantum computation [7].

Quantum Phase Transition.— By tuning the interaction U_n , we can drive a quantum phase transition from the non-Abelian state to other quantum phases[15, 53]. A natural question is how the MESs and related modular \mathcal{S} matrix evolve around the quantum phase transition region. Here we study the SQ lattice model at $\nu = 1$ as example, in which the quantum phase transition occurs around $0.3 < U_2^c < 0.4$ [53]. In the MR phase ($U_2 = 0.1$), we find that the entropy profile of superposition state has three valleys labeled by I, II and III, as shown in Fig. 4(a). The three orthogonal MESs are located in the above three valleys, respectively. The resulting modular matrix remains close to the theoretical one for the MR

state: $\mathcal{S} = \frac{1}{1.965} \begin{pmatrix} 1.000 & 1.041 & 1.316 \\ 1.006 & 0.888 & -1.448 \\ 1.334 & -1.440 & 0.028 \end{pmatrix}$. We have also

checked that the \mathcal{S} faithfully represents the quasiparticle information for the whole phase region at $U_2 \leq 0.3$. After the quantum phase transition at $U_2 = 0.5 > U_2^c$, we can only find two entropy valleys in entropy map, as labeled by I,II in Fig. 4(b), which relates to the first two MESs. The third possible MES state (labeled by white arrow) determined by the orthogonality relation, actually is not a local minimum. We continue to use these MESs as basis states to obtain the mod-

ular \mathcal{S} matrix: $\mathcal{S} = \frac{1}{3.731} \begin{pmatrix} 1.000 & 2.873 & 2.037 \\ 2.899 & 0.750 & 2.354 \\ 2.015 & 2.354 & 2.082 \end{pmatrix}$, which

deviates significantly from the MR \mathcal{S} matrix. In particular, the quasiparticle fusion rule and statistics has changed with \mathcal{S}_{33} deviating from zero, which demonstrates the disappearance of the MR phase.

Summary and discussion.— We have numerically studied the non-Abelian quasiparticle statistics in the lattice boson models which manifest the MR and RR non-Abelian states at filling factor $\nu = 1$ and $\nu = 3/2$, respectively. Our work provides the first convincing demonstration of quasiparticle fusion rules and statistics in microscopic topological band models. The obtained modular \mathcal{S} matrix faithfully represents Majorana and Fibonacci quasiparticle statistics includ-

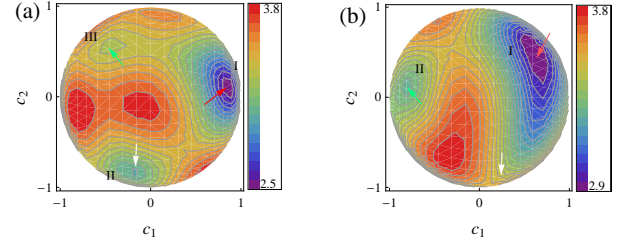


FIG. 4: (Color online) The entropy of superposition state $|\Psi\rangle$ in $c_1 - c_2$ space ($c_3 = \sqrt{1 - c_1^2 - c_2^2}$) for (a) $U_2 = 0.1$ and (b) $U_2 = 0.5$ by setting optimized ϕ_2, ϕ_3 at $\nu = 1$ on the SQ lattice.

ing the quantum dimension for each quasiparticle and the fusion rules, which fully support that the each MES is the eigenstate with a definite type of quasiparticle. We are currently developing a numerical method in DMRG simulations to target different MESs by projecting out the previously identified lower MESs, which we believe will become a useful tool for detecting the full information of the topological order through modular matrix simulation in larger interacting systems [56].

Acknowledgements.— This work is supported by the US NSF under grants DMR-0906816 (WZ,SSG), and by the Princeton MRSEC Grant DMR-0819860 (FDMH), and the Department Of Energy Office of Basic Energy Sciences under Grant No. DE-FG02-06ER46305 (DNS). DNS also acknowledges the travel support by the Princeton MRSEC.

-
- [1] R. B. Laughlin, Phys. Rev. Lett. **50**, 1395 (1983).
 - [2] G. Moore and N. Read, Nucl. Phys. B **360**, 362 (1991).
 - [3] M. Greiter, X. G. Wen and F. Wilczek, Phys. Rev. Lett. **66**, 3205 (1991).
 - [4] N. Read and E. Rezayi, Phys. Rev. B **59**, 8084 (1999).
 - [5] A. Y. Kitaev, Ann. Phys. **303**, 2 (2003).
 - [6] S. Das Sarma, M. Freedman and C. Nayak, Phys. Rev. Lett. **94**, 166802 (2005).
 - [7] C. Nayak, S. H. Simon, A. Stern, M. Freedman and S. D. Sarma, Rev. Mod. Phys. **80**, 1083 (2008).
 - [8] R. Willett, J. P. Eisenstein, H. L. Stormer, D. C. Tsui, A. C. Gosard and J. H. English, Phys. Rev. Lett. **59**, 1776 (1987).
 - [9] J. S. Xia, W. Pan, C. L. Vicente, E. D. Adams, N. S. Sullivan, H. L. Stormer, D. C. Tsui, L. N. Pfeiffer, K. W. Baldwin, and K. W. West, Phys. Rev. Lett. **93**, 176809 (2004).
 - [10] R. H. Morf, Phys. Rev. Lett. **80**, 1505 (1998).
 - [11] E. H. Rezayi and F. D. M. Haldane, Phys. Rev. Lett. **84**, 4685 (2000).
 - [12] E. H. Rezayi and N. Read, Phys. Rev. B **79**, 075306 (2009).
 - [13] N. R. Cooper, N. K. Wilkin, and J. M. F. Gunn, Phys. Rev. Lett. **87**, 120405 (2001).
 - [14] N. R. Cooper and J. Dalibard, Phys. Rev. Lett. **110**, 185301 (2013).
 - [15] Y. F. Wang, H. Yao, Z. C. Gu, C. D. Gong, and D. N. Sheng, Phys. Rev. Lett. **108**, 126805 (2012).
 - [16] F. D. M. Haldane, Phys. Rev. Lett. **61**, 2015 (1988).
 - [17] E. Kapit and E. Mueller, Phys. Rev. Lett. **105**, 215303 (2010).
 - [18] E. Tang, J. W. Mei and X. G. Wen, Phys. Rev. Lett. **106**, 236802 (2011).

- (2011).
- [19] T. Neupert, L. Santos, C. Chamon and C. Mudry, Phys. Rev. Lett. **106**, 236804 (2011).
 - [20] K. Sun, Z. C. Gu, H. Katsura and S. Das Sarma, Phys. Rev. Lett. **106**, 236803 (2011).
 - [21] D. N. Sheng, Z. C. Gu, K. Sun and L. Sheng, Nature Commun. **2**, 389 (2011).
 - [22] N. Regnault and B. A. Bernevig, Phys. Rev. X **1**, 021014 (2011).
 - [23] Y.-F. Wang, Z.-C. Gu, C.-D. Gong and D. N. Sheng, Phys. Rev. Lett. **107**, 146803 (2011).
 - [24] E. Verlinde, Nucl. Phys. B **300**, 360176 (1988).
 - [25] X. G. Wen, Int. J. Mod. Phys. B **4**, 239 (1990).
 - [26] S. Dong, E. Fradkin, R. G. Leigha and S. Nowling, JHEP 05, 016 (2008).
 - [27] E. Rowell, R. Stong, Z. H. Wang, Comm. Math. Phys. **292**, 343 (2009).
 - [28] P. Fendley, M. P. A. Fisher and C. Nayak, J.Stat.Phys. **126**, 1111(2007).
 - [29] P. Bonderson, K. Shtengel and J. K. Slingerland, Phys. Rev. Lett. **97**, 016401 (2006).
 - [30] E. Ardonne, E. J. Bergholtz, J. Kailasvuori and E. Wikberg, J. Stat. Mech. 04, 016 (2008).
 - [31] F. A. Bais and J. C. Romers, New J. Phys. **14**, 035024 (2012).
 - [32] X. G. Wen, arXiv:1212.5121.
 - [33] A. Kitaev and J. Preskill, Phys. Rev. Lett. **96**, 110404 (2006).
 - [34] M. Levin and X.-G. Wen, Phys. Rev. Lett. **96**, 110405 (2006).
 - [35] G.S. Jeon, K.L. Graham, and J.K. Jain, Phys. Rev. Lett. **91**, 036801 (2003).
 - [36] Y. Tserkovnyak and S.H. Simon, Phys. Rev. Lett. **90**, 016802 (2003).
 - [37] M. Baraban, G. Zikos, N. Bonesteel, and S.H. Simon, Phys. Rev. Lett. **103**, 076801 (2009).
 - [38] E. Prodan and F.D.M. Haldane, Phys. Rev. B **80**, 115121 (2009).
 - [39] V. Lahtinen and J.K. Pachos, New J. Phys. **11**, 093027 (2009).
 - [40] A.T. Bloukbasi and J. Vala, New J. Phys. **14**, 045007 (2012).
 - [41] E. Kapit, P. Ginsparg, and E. Mueller, Phys. Rev. Lett. **108**, 066802 (2012).
 - [42] M. Haque, O. Zozulya, and K. Schoutens, Phys. Rev. Lett. **98**, 060401 (2007).
 - [43] S. V. Isakov, M. B. Hastings and R. G. Melko, Nat. Phys. **7**, 772 (2011).
 - [44] H. C. Jiang, Z. H. Wang and L. Balents, Nat. Phys. **8**, 902 (2012).
 - [45] H. Li and F. D. M. Haldane, Phys. Rev. Lett. **101**, 010504 (2008).
 - [46] A. M. Lauchli, E. J. Bergholtz, J. Suorsa and M. Haque, Phys. Rev. Lett. **104**, 156404 (2010).
 - [47] Y. Zhang, T. Grover, A. Turner, M. Oshikawa and A. Vishwanath, Phys. Rev. B **85**, 235151 (2012).
 - [48] L. Cincio and G. Vidal, Phys. Rev. Lett. **110**, 067208 (2013).
 - [49] H. H. Tu, Y. Zhang, and X. L. Qi, arxiv:1212.6951.
 - [50] M. P. Zaletel, R. S. K. Mong, and F. Pollmann, Phys. Rev. Lett. **110**, 236801 (2013).
 - [51] W. Zhu, D. N. Sheng and F. D. M. Haldane, Phys. Rev. B **88**, 035122 (2013).
 - [52] Y. Zhang and A. Vishwanath, Phys. Rev. B **87**, 161113(R).
 - [53] Supplemental Materials.
 - [54] B. A. Bernvig and N. Regnault, Phys. Rev. B **85**, 075128 (2012).
 - [55] A. Feiguin, S. Trebst, A. W. W. Ludwig, M. Troyer, A. Kitaev, Z. H. Wang, and M. H. Freedman, Phys. Rev. Lett. **98**, 160409 (2008).
 - [56] D. N. Sheng, *et. al*, in preparation.

SUPPLEMENTAL MATERIALS FOR: “IDENTIFYING NON-ABELIAN TOPOLOGICAL ORDER THROUGH MINIMAL ENTANGLED STATES”

In this supplemental material, we study the quasiparticle statistics of the non-Abelian Moore-Read (MR) state on the square (SQ) lattice at filling factor $\nu = 1$. First, we find convincing evidence that the phase at filling factor $\nu = 1$ manifests the MR state. Then we search for the minimal entangled states (MESSs) in the groundstate manifold and determine the modular \mathcal{S} matrix.

Low-energy Spectrum at $\nu = 1$.— The Hamiltonian has been described in the main text and we select $U_3 = \infty$ here so that the system is effectively equivalent to a spin-1 system. Low-energy spectrum versus different U_2 on the 4×4 SQ lattice is shown in Fig.5(a). When $U_2 = 0.0$, we find a groundstate manifold (GSM) with three exact degenerate lowest eigenstates. With increasing U_2 , the exact degeneracy of GSM is destroyed and two groundstates from the GSM will evolve into the excited spectrum. We have also obtained numerical results from larger lattice size (4×5 and 4×6) and have confirmed that the above picture is qualitatively correct. To confirm the robustness of this Fractional Quantum Hall (FQH) phase, we also introduce two boundary phases θ_1 and θ_2 for generalized boundary conditions and calculate the Chern number (Berry phase in units of 2π) of GSM. The three groundstates maintain their quasi-degeneracy and are well separated from the low-energy excitation spectrum upon tuning the boundary phases (Fig.5(b)). Moreover, the three-fold GSM is found to share a total Chern number $C = 3$. Furthermore, we study the Particle entanglement spectrum (PES) of the three-fold GSM (Fig.5(c)). PES reveals a gap at $U_2 < 0.4$ and the number of states below this gap exactly agrees with the number of quasihole excitations in a MR state based on the generalized Pauli principle that no more than two bosons occupy two consecutive orbitals [54]. Thus we reach

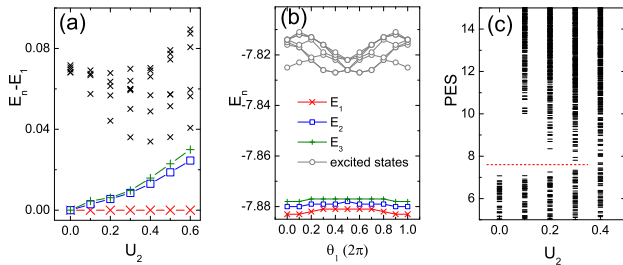


FIG. 5: (Color online) (a) Low-energy spectrum $E_n - E_1$ versus the U_2 ($U_3 = \infty$) on a 4×4 SQ lattice at $\nu = 1$. Three lowest eigenvalues are labeled by blue square, red cross and green cross. (b) Low-energy spectra versus boundary phase θ_1 at a fixed $\theta_2 = 0$ for $U_2 = 0.1$. (c) Particle entanglement spectrum (PES) for tracing out 4 bosons. There are 170 states below the PES gap (red dashed line) for $U_2 < 0.4$, in good agreement with the counting of quasihole excitations in MR state.

the conclusion that the three-fold GSM at $\nu = 1$ mimics non-Abelian MR state at $U_2 < 0.4$. The PES gap disappears for $U_2 \sim 0.4$ signaling the quantum phase transition from the non-Abelian MR state to a topological trivial state [15].

MESSs and modular matrix at $\nu = 1$.— We denote the three groundstates from ED calculation as $|\xi_j\rangle$, (with $j = 1, 2, 3$). Now we form the general superposition state as,

$$|\Psi_{(c_1, c_2, \phi_2, \phi_3)}\rangle = c_1|\xi_1\rangle + c_2e^{i\phi_2}|\xi_2\rangle + c_3e^{i\phi_3}|\xi_3\rangle$$

where $c_1, c_2, c_3, \phi_2, \phi_3$ are real superposition parameters. For each state $|\Psi\rangle$, we construct the reduced density matrix and obtain the corresponding entanglement entropy. We optimize values of $c_i \in [0, 1]$ and $\phi_i \in [0, 2\pi]$ to minimize the entanglement entropy. In Fig. 6(a-b), we show the entropy profile at optimized parameters (ϕ_2^o, ϕ_3^o) for MESSs. In Fig. 6(a), it is found several peaks (entropy valleys) in $c_1 - c_2$ space and the three nearly orthogonal MESSs are determined as labeled by arrows. In Fig. 6(b), it is shown the entropies of states in the parameter space orthogonal to the first MES (red arrow). The second and the third MESSs are indeed located in the separated entropy valleys, respectively. Here we find that the entropies corresponding to the three MESSs are different from each other (as list in Table-I in main text). The entropy difference between the first MES and the second MES may result from the finite-size effect. To identify the emergence of non-Abelian quasiparticles, we calculate the modular matrix and obtain the quasiparticle statistics as below.

With the help of MESSs, we obtain the modular matrix

$$\mathcal{S} \approx \frac{1}{1.961} \begin{pmatrix} 1.000 & 1.025 & 1.373 \\ 0.929 & 0.920 & -1.431 \\ 1.392 & -1.376 & 0.037 \end{pmatrix} \quad (6)$$

, which is close to the prediction of $SU(2)_2$ Chern-Simons theory: $\mathcal{S} = \frac{1}{2} \begin{pmatrix} 1 & 1 & \sqrt{2} \\ 1 & 1 & -\sqrt{2} \\ \sqrt{2} & -\sqrt{2} & 0 \end{pmatrix}$. We extract the three quasiparticle quantum dimension as $d_{\mathbb{I}}^{SQ} = 1.000$, $d_{\psi}^{SQ} \approx$

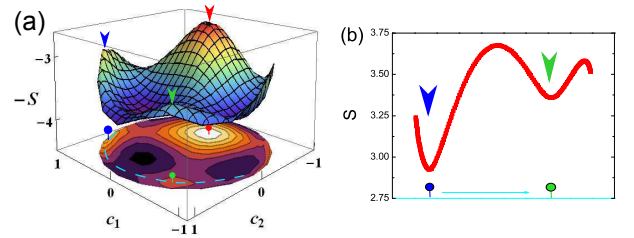


FIG. 6: (Color online) (a) Surface and contour plots of entanglement entropy $-S$ of $|\Psi_{c_1, c_2, \phi_2, \phi_3}\rangle$ on 4×4 SQ lattice at $\nu = 1$. We show entropy profile versus c_1, c_2 ($c_3 = \sqrt{1 - c_1^2 - c_2^2}$) by setting optimized $\phi_2^o = 0.24\pi$, $\phi_3^o = 0.52\pi$. Three nearly orthogonal MESSs are marked by red, green and blue arrows (dots) in surface (contour) plot. The cyan dashed line represents the states orthogonal to the first MES (red dot). (b) Entropy for the states along the cyan dashed line as shown in (a). All calculations are for partition along cut-I.

0.929, $d_\sigma^{SQ} \approx 1.392$ and the total quantum dimension $\mathcal{D}^{SQ} \approx 1.961$. Combined with the fusion rule of the third type of quasiparticle σ : $\sigma \times \sigma \approx 0.951\mathbb{1} + 0.959\psi + 0.004\sigma$ (as

shown in the main text), we confirm that σ behaves as the non-Abelian Majorana quasiparticle.